

of extremely old, recycled pulsars (in fact, the mystery is the presence of some anomalously young pulsars, see e.g. [Boyles et al. 2011](#), a likely solution to this problem is the recent disruption of LMXBs, see [Verbunt & Freire 2014](#)). Although the total number of globular cluster pulsars accounts for about 5% of the total pulsar population, the millisecond pulsars (MSPs, here defined as those having a spin period $P < 10$ ms) that are found in GCs account for about 40% of the known MSP population².

This large population of MSPs include some of the most extreme pulsars and systems known. Among these are extremely recycled MSPs (e.g., PSR J1748–2446ad in Terzan 5; [Hessels et al. 2006](#)), extremely compact binaries (e.g., PSR J0024–7204R in 47 Tucanae; [Freire et al. 2017](#)), extremely energetic pulsars, with very high γ -ray luminosities (e.g. PSR B1820–30 in NGC 6624, [Freire et al. 2011a](#); and PSR B1821–24 in M28, [Johnson et al. 2013](#)) and a radio pulsar in a “redback” system that changes into an accreting X-ray MSP and back to radio in timescales of weeks ([Papitto et al. 2013](#)).

Among the most exotic systems in GCs are a small group of MSPs in highly eccentric binaries with massive companions: PSR J1835–3259A in NGC 6652 ([DeCesar et al. 2015](#)), PSR J1807–2500B ([Lynch et al. 2012](#)), and PSR J0514–4002A in NGC 1851, ([Freire et al. 2004, 2007](#)). These systems are so unlike anything seen in the Galaxy that they are almost certainly the result of *secondary exchange encounters*, i.e., exchange encounters that happen after the pulsar is recycled by a lower-mass companion, which is ejected and exchanged by a much more massive compact object. This is only likely to happen (and has only been observed) in GCs with a large interaction rate *per binary* ([Verbunt & Freire 2014](#)). A confirmation of this is PSR B2127+11C, a double neutron star system in the core-collapsed globular cluster M15 ([Jacoby et al. 2006](#)). Although it superficially resembles a “normal” double neutron star like those found in the Galaxy, it was recognized at an earlier stage that it too must be the result of a secondary exchange interaction ([Prince et al. 1991](#)).

These systems are the ultimate example of a non-standard evolutionary path; they suggest that even more exotic systems, like double MSP and MSP-black hole systems, might be discovered in the future.

1.1 NGC 1851A

One of these systems, PSR J0514–4002A, consists of a 4.99-ms pulsar in orbit around a massive companion every 18.8 days in a very eccentric ($e = 0.89$) orbit. It is located in the globular cluster NGC 1851, henceforth we designate this system as NGC 1851A. The pulsar was discovered at 327 MHz with the Giant Metrewave Radio Telescope (GMRT) located near Khodad, India, in the context of a small low-frequency survey for pulsars in GCs ([Freire et al. 2004](#)).

Subsequent follow-up observations with the Green Bank Telescope allowed for the derivation of a phase-connected

timing solution ([Freire et al. 2007](#)). As suggested by earlier GMRT interferometric images ([Freire et al. 2004](#)), the pulsar is at about one core radius from the centre of NGC 1851. By measuring the rate of periastron advance, the authors were able to derive the total mass of the system ($M_{\text{tot}} = 2.453(14) M_{\odot}$) and obtain an upper limit on the mass of the pulsar ($M_{\text{p}} < 1.5 M_{\odot}$) and a lower limit on that of the companion ($M_{\text{c}} > 0.96 M_{\odot}$). Although the data were not sufficient to detect additional post-Keplerian (PK) effects, which would give access to the individual masses of the binary components, [Freire et al. \(2007\)](#) envisaged a measurement of the Einstein delay (γ), and, depending on the system inclination, of the Shapiro delay, in a not too distant future.

1.2 Motivation and structure of the paper

After a hiatus of about one decade, new observations of NGC 1851A were motivated by the major upgrade recently undergone by the GMRT ([Gupta et al. 2017](#)). In a first stage, issues with the timing stability have been solved, allowing for precise timing of MSPs. Later, the whole array has been upgraded with new receivers and electronics. Compared to its original configuration, the upgraded GMRT (hereafter, uGMRT) delivers up to a factor of three better sensitivity. This is achieved mainly by means of new wide-band receivers, which provide an almost seamless frequency coverage from ~ 50 to ~ 1450 MHz, and a modern digital back-end system ([Reddy et al. 2017](#)) that allows a maximum instantaneous bandwidth of 400 MHz with real-time coherent de-dispersion. The latter feature is critical to maximize the sensitivity to far, highly dispersed GCs, when observed at very low frequencies.

At the same time, detailed simulations suggested that a dense timing campaign over one orbit should be able to determine at least the relativistic γ parameter with enough accuracy to measure the component masses to an uncertainty of about $0.05 M_{\odot}$. Furthermore, a more sparse set of timing measurements spread over one year would enable a precise measurement of the proper motion of the system. This, as shown below, is of great importance for a proper interpretation of the measurement of γ .

Thus, the new capabilities of the uGMRT offered the chance to finally measure the mass of NGC 1851A and its companion with good precision. Such a measurement is extremely valuable, not only for improving the statistics of MSP mass measurements (still very small in GCs), but also to investigate the nature of the companion. As we will see below, our measurements indicate that this companion could well be another neutron star (NS). Since the system very likely formed in an exchange encounter, the nature of this companion cannot be elucidated by arguments based on stellar evolution.

The remainder of the paper is organized as follows: In section 2, we describe the new uGMRT timing observations and how the resulting data were reduced. In section 3, we present the results of our timing analysis, with a particular emphasis on the measurements of the PK parameters and their likely kinematic contaminants; this will be especially relevant for the measurement of the variation of the orbital period (\dot{P}_b) and γ . In section 4, we perform a self-consistent Bayesian analysis of the orbital orientation space

² As of 2018 April, see the PSRCAT pulsar catalog at <http://www.atnf.csiro.au/research/pulsar/psrcat> ([Manchester et al. 2005](#))

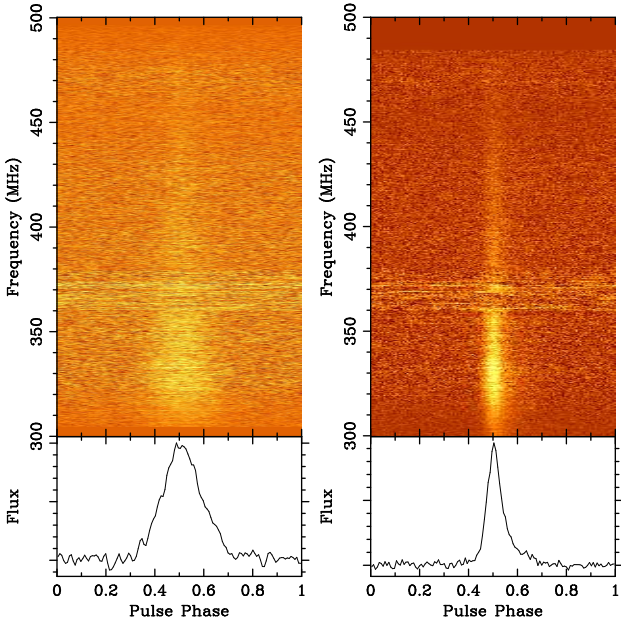


Figure 1. Observation of NGC 1851A as taken with the 250–500 MHz (Band 3) receiver of the uGMRT on 2017 November 14 simultaneously in PA mode (left) and CDP mode (right). Top panels: intensity as a function of pulse phase (x -axis) and time (y -axis). Bottom panels: corresponding integrated pulse profile. Thanks to the coherent de-dispersion available in CDP mode, the pulse profile of NGC 1851A is much narrower than in PA mode, resulting in far more precise timing. Radio frequency interference from the Mobile User Objective System (MUOS) satellite system is visible in the 360–380 MHz band.

to determine the likely inclination ranges and the masses of the components. Since the companion has a mass that is compatible with it being a NS, it might also be a pulsar. For this reason, in section 5 we search for pulsations from the companion, globular cluster NGC 1851. Finally, in section 6, we summarize our findings, elaborate on the nature of the companion star and discuss some interesting long-term prospects.

2 OBSERVATIONS AND DATA REDUCTION

2.1 Observations

We used the uGMRT to observe NGC 1851A at 20 different epochs, from 2017 April to 2018 March (Table 1). The observing strategy was designed with two main objectives in mind: a) improve the measurements of the proper motion and spin-down parameters, and b) possibly measure additional PK parameters, such as the Einstein delay and the Shapiro delay. For the first purpose, we carried out ~ 40 -min-long observations with a roughly monthly cadence. For the second purpose, we carried out a single dense orbital campaign in 2017 May, during which the pulsar was observed on ten different occasions within the ~ 18.8 d of its orbit, with longer scans as the pulsar was approaching periastron. All observations were made with the 14 antennas of the uGMRT central array, using the 250–500 MHz receivers (uGMRT Band 3). After summing the two polarizations, the data were 16-bit digitized and recorded in search mode by

the GMRT Wideband Backend (GWB, Reddy et al. 2017), with a total bandwidth of 200 MHz centered at a frequency of 400 MHz.

Until 2017 August, the data were taken in Phased Array (PA) mode only, with a sampling time of $81.92 \mu\text{s}$ and 2048, ~ 0.0977 -MHz wide frequency channels. Given its dispersion measure (DM) of $\sim 52.14 \text{ pc cm}^{-3}$, the signal of NGC 1851A had a dispersive smearing across each channel of $338 \mu\text{s}$ at the top (500 MHz) of the band, and of 1.565 ms at the bottom (300 MHz) of the band. These translated into an effective resolution of $348 \mu\text{s}$ and 1.567 ms at the top and the bottom of the band, respectively.

From 2017 September, the new real-time coherent de-dispersion (CDP) mode of the GWB became available. The last six observations made from 2017 October to 2018 March were therefore made using the PA and CDP modes simultaneously. In CDP mode, the observing band was divided into 512 frequency channels, which were coherently de-dispersed at the nominal DM of NGC 1851A. Thanks to this, the chosen sampling time of $10.24 \mu\text{s}$ also corresponds to the effective time resolution of the CDP data. The much higher quality provided by the CDP data over the PA data is evident from Fig. 1, where we show a single observation of NGC 1851A as resulting from the two different modes. The lack of intra-channel dispersive smearing in CDP mode results in a much narrower pulse profile. Its shape is thus much closer to the intrinsic one, likely only slightly smeared by scattering.

2.2 Data reduction

The newly taken uGMRT search-mode data were first folded with the `prepfold` routine of a slightly modified version of the classic branch³ of the PRESTO⁴ (Ransom 2001) pulsar search package, using the best NGC 1851A ephemeris available. The so produced PRESTO folded archives were then converted into PSRFITS format using the `psrconv` routine of the PSRCHIVE⁵ pulsar software package (van Straten et al. 2012) and then carefully cleaned from radio frequency interference (RFI). All the PA and CDP archives were then separately summed together to produce a high signal-to-noise (S/N) PA integrated profile, and a high-S/N CDP integrated profile, respectively. Both profiles were then smoothed with a Wavelet transform (using the `psrsmooth` routine of PSRCHIVE) so as to obtain two noise-free template profiles to be used with the PA and CDP datasets, respectively. The use of two different templates for the different datasets is justified by the large differences in the observed profile shape of NGC 1851A in the PA and CDP data (Fig. 1). Each noise-free template was then cross-correlated in the Fourier domain (Taylor 1992) against the folded archives of the relative dataset to derive topocentric pulse times of arrival (ToAs). Because the time stamps of the CDP data are known to have a positive offset of 0.67108864 seconds with respect to those of the PA data, we took this difference into

³ The classic branch of PRESTO is currently the only version capable of dealing with the GMRT data format.

⁴ <http://www.cv.nrao.edu/~sransom/presto>

⁵ <http://psrchive.sourceforge.net>

Table 1. List of the recent observations of NGC 1851A made with the uGMRT. All observations were carried out with the 250–500 MHz receiver (Band 3), GWB as backend, with 200 MHz of bandwidth. The dates and epochs reported are referred to the start time of the observation in UTC time standard. PA: Phased Array mode; CDP: Coherent De-dispersion mode.

Date	Epoch (MJD)	Mode	Length (min)	Sampling time (μ s)	Number of channels	Mean anomaly range (deg)	Notes
2017 Apr 29	57872	PA	25	81.92	2048	74.00 – 74.33	
2017 May 07	57880	PA	40	81.92	2048	223.75 – 224.28	
2017 May 09	57882	PA	33	81.92	2048	265.41 – 265.84	
2017 May 10	57883	PA	40	81.92	2048	284.54 – 285.07	
2017 May 11	57884	PA	40	81.92	2048	303.76 – 304.29	
2017 May 13	57886	PA	105	81.92	2048	340.82 – 342.50	
2017 May 14	57887	PA	275	81.92	2048	357.45 – 361.11	Periastron passage
2017 May 15	57888	PA	96	81.92	2048	17.83 – 19.11	
2017 May 17	57890	PA	53	81.92	2048	58.58 – 59.29	
2017 May 19	57892	PA	40	81.92	2048	96.79 – 97.32	
2017 May 22	57895	PA	50	81.92	2048	150.22 – 150.88	
2017 Jun 10	57914	PA	40	81.92	2048	155.93 – 156.46	
2017 Jul 12	57946	PA	40	81.92	2048	45.63 – 46.17	
2017 Aug 19	57984	PA	40	81.92	2048	53.23 – 53.77	
2017 Oct 26	58052	PA / CDP	40	81.92 / 10.24	2048 / 512	273.68 – 274.22	
2017 Nov 14	58071	PA / CDP	26	81.92 / 10.24	2048 / 512	294.65 – 295.00	
2017 Dec 14	58101	PA / CDP	40	81.92 / 10.24	2048 / 512	148.65 – 149.19	
2018 Jan 13	58131	PA / CDP	40	81.92 / 10.24	2048 / 512	359.94 – 360.47	Periastron passage
2018 Feb 15	58164	PA / CDP	40	81.92 / 10.24	2048 / 512	271.41 – 271.94	
2018 Mar 15	58192	PA / CDP	40	81.92 / 10.24	2048 / 512	88.18 – 88.71	

account by subtracting the value from all the CDP ToAs⁶. Also, the PA and CDP template profiles were aligned in phase, using the profile peak as the reference point, so as to avoid the introduction of any additional phase offsets. In this way, the PA and CDP ToAs were directly comparable and no arbitrary offset between the two datasets was needed⁷.

The new uGMRT ToAs were then used to extend the pulsar ephemeris published by Freire et al. (2007) to the present time, using the TEMPO⁸ pulsar timing package. When doing so, the ToAs are first referred to the Terrestrial Time standard of the Bureau International des Poids et Mesures (BIPM). In order to subtract the motion of the radio telescope around the Earth’s centre, TEMPO uses the International Earth Rotation Service tables and the known coordinates of the telescope. The Earth’s motion relative to the Solar System barycentre (SSB) was also subtracted by TEMPO using the DE 430 Solar System ephemeris derived by the Jet Propulsion Laboratory (Folkner et al. 2014). The resulting timing parameters are presented in Barycentric Dynamical Time (TDB).

We used two of the TEMPO orbital models to analyze the data, all based on the description of Damour & Deruelle (1985, 1986). The first is the “DDFWHE” model (Weisberg & Huang 2016), which is based on theory-independent “DD” model, but with the orthometric parameterization of the Shapiro delay described by Freire & Wex (2010). The second is the “DDK” model, which will later be used in the

Bayesian analysis outlined in section 4. This is, again, based on the DD model but takes into account the kinematic effects described by Kopeikin (1995, 1996) and was implemented in TEMPO by van Straten & Bailes (2003).

3 RESULTS

The timing parameters for NGC 1851A are presented in Table 2. The ToA residuals (calculated as observed ToA – prediction of the timing solution for the same rotation number) are displayed graphically in Fig. 2. These show no clear systematic trends, which suggests that the ephemeris in Table 2 accounts well for the spin and motion of the pulsar.

We will now discuss the astrometric, spin and binary parameters in this solution. However, before we proceed, we must remark that some parameters, like the second spin frequency derivative, the proper motion and the orbital period derivative, are still subject to change, showing significant differences with every new observation added. Therefore, their values must be interpreted with caution; they will be discussed in more detail in a future publication after further timing provides stable measurements for those parameters. Other parameters, particularly those used to derive the masses of the components, appear to be much more robust. For this reason, the bulk of the discussion will be centered on the mass measurements.

The main new observational result in this section is the detection of the Einstein delay γ (see section 3.6). Another highlight is the detailed interpretation of γ , in particular the study of its correlation with the rate of change of the projected semi-major axis of the pulsar orbit, \dot{x} , in sections 3.7 to 3.9.

⁶ This was done by using the TEMPO’s TIME statement in the ToA file.

⁷ Although the different profile shapes could also introduce an additional offset between the PA and CDP ToAs, the timing solutions obtained with and without accounting for such an offset proved to be compatible within $1\text{-}\sigma$.

⁸ <http://tempo.sourceforge.net>

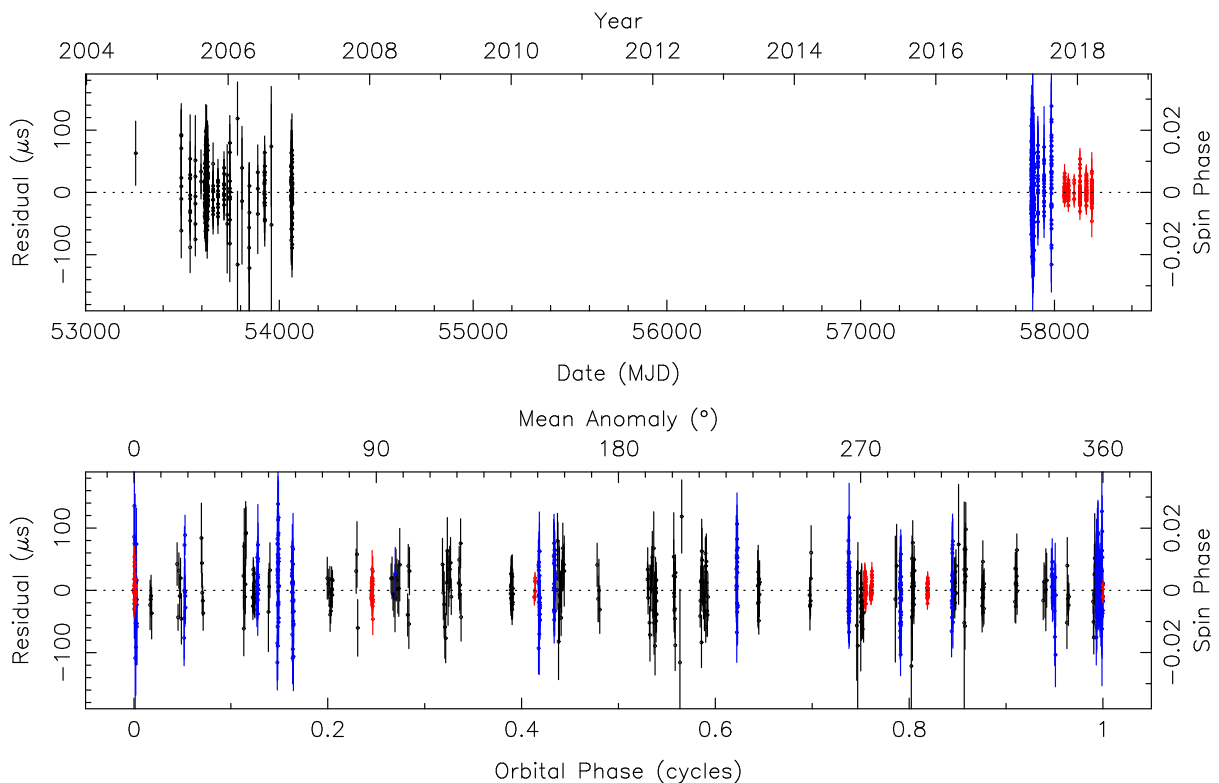


Figure 2. Timing residuals for NGC 1851A, obtained with the DDFWHE timing solution listed in Table 2. *Top:* ToA residuals as a function of the epoch, with the 10-year gap in observations evident. *Bottom:* ToA residuals as a function of the orbital phase, with phase 0 denoting periastron. The residual $1\text{-}\sigma$ uncertainties are indicated by vertical error bars. Black indicates the earlier GBT timing, blue the uGMRT data taken in phased array (PA) mode, and red the uGMRT data in coherent de-dispersion (CDP) mode. Note the marked improvement of the CDP data compared to the PA mode.

3.1 Proper motion: transverse velocity relative to NGC 1851

Contrary to the first timing solution published by Freire et al. (2007), which was limited by a ~ 2 -yr dataset, the much longer time baseline spanned by our ToAs allowed us to precisely measure the pulsar’s proper motion. The latter amounts to $\mu_\alpha = +5.19 \pm 0.22 \text{ mas yr}^{-1}$ in right ascension and $\mu_\delta = -0.56 \pm 0.25 \text{ mas yr}^{-1}$ in declination. This can be compared to the astrometric measurement of the proper motion of the cluster as a whole, as recently published by the GAIA Collaboration with their Data Release 2 (Gaia Collaboration et al. 2018). For NGC 1851 they report $\mu_\alpha = +2.1308 \pm 0.0037 \text{ mas yr}^{-1}$ and $\mu_\delta = -0.6220 \pm 0.0040 \text{ mas yr}^{-1}$. The motion of the pulsar relative to the cluster is therefore $\Delta\mu_\alpha = +3.06 \pm 0.22 \text{ mas yr}^{-1}$ and $\Delta\mu_\delta = +0.06 \pm 0.25 \text{ mas yr}^{-1}$ and it is graphically shown in Fig. 3. Given the distance to NGC 1851 of $d = 12.1 \pm 0.2 \text{ kpc}$ (Gaia Collaboration et al. 2018), this translates into a relative linear velocity of $\sim 175 \pm 13 \text{ km/s}$. This is more than four times larger than the cluster’s central escape velocity ($\sim 42.9 \text{ km/s}$, Baumgardt & Hilker 2018), hence it would imply that the pulsar is not bound to NGC 1851. However, we point out that this result is a direct consequence of the large discrepancy between the proper motion of the pulsar, measured by radio timing, and that of the cluster, measured by the much more precise GAIA’s astrometry. Such a discrepancy may be due to covariances between the proper motion

and the pulsar’s spin-down parameters, as the latter can be heavily affected by the cluster’s gravitational potential (see discussion in Section 3.3). Considering the 10-yr gap in our timing data, and the fact that the recent one year of data was taken with two different back-ends, it is too early to draw any firm conclusions. Further radio observations of NGC 1851A over the next few years will be necessary before we are able to accurately measure higher order spin period derivatives, which will in turn improve the measurement of the pulsar’s proper motion.

3.2 Keplerian orbital parameters

As already discussed by Freire et al. (2004) and Freire et al. (2007), NGC 1851A is, among binary MSPs, an unusually eccentric system, $e = 0.8879771(11)$, the second highest after PSR J1835–3259A in NGC 6652, with $e = 0.968(5)$ (DeCesar et al. 2015). Furthermore, it must have an unusually massive companion, since it has a high mass function, f :

$$f = \frac{(M_c \sin i)^3}{M_{\text{tot}}^2} = \frac{4\pi^2 x^3}{T_\odot P_b^2} = 0.1454196(33) M_\odot, \quad (1)$$

where M_{tot} is total system mass, x is the projection of the semi-major axis of the pulsar’s orbit along the line of sight in light-seconds (lt-s), P_b is the orbital period of the binary, and $T_\odot = GM_\odot c^{-3} = 4.925490947 \mu\text{s}$ is a solar mass (M_\odot)

Table 2. Timing parameters for PSR J0514–4002A

Observation and data reduction parameters	
Reference Epoch (MJD)	53623.1551
Span of timing data (MJD)	53258 – 58192
Number of ToAs	939
Solar wind parameter, n_0 (cm ⁻³)	10
Overall residual rms (μ s)	20.9
RMS residual for GBT data (μ s)	30.2
RMS residual for GMRT PA data (μ s)	36.1
RMS residual for GMRT CDP data (μ s)	11.4
χ^2	927.31
Reduced χ^2	1.008
Astrometric and spin parameters	
Right ascension, α (J2000)	05:14:06.69271(20)
Declination, δ (J2000)	–40:02:48.8930(19)
Proper motion in α , μ_α (mas yr ⁻¹)	5.19(22)
Proper motion in δ , μ_δ (mas yr ⁻¹)	–0.56(25)
Parallax, ϖ (mas)	0.0826
Spin frequency, ν (Hz)	200.37770740535(10)
First derivative of ν , $\dot{\nu}$ (10 ⁻¹⁷ Hz s ⁻¹)	–2.8(5)
Second derivative of ν , $\ddot{\nu}$ (10 ⁻²⁴ Hz s ⁻²)	–1.533(27)
Dispersion measure, DM (pc cm ⁻³)	52.14016(37)
Binary parameters	
Orbital period, P_b (days)	18.785179217(19)
Projected semi-major axis, x (lt-s)	36.29028(27)
Epoch of periastron, T_0 (MJD)	53623.15508797(35)
Orbital eccentricity, e	0.8879771(11)
Longitude of periastron, ω (°)	82.3402(31)
Rate of advance of periastron, $\dot{\omega}$ (deg yr ⁻¹)	0.0129592(16)
Einstein delay, γ (s)	0.0216(9)
Derivative of P_b , \dot{P}_b (10 ⁻¹² s s ⁻¹)	22(9)
Orthometric amplitude of Shapiro delay, h_3 (μ s)	0.2(13)
Orthometric ratio of Shapiro delay, ς	0.498 ^a
Derived parameters	
Magnitude of proper motion, μ (mas yr ⁻¹)	5.22(22)
PA of proper motion, Θ_μ (deg, J2000)	96.2(28)
PA of proper motion, Θ_μ (deg, Galactic)	14.8(28)
Spin period, P (ms)	4.9905751141121(24)
Spin period derivative, \dot{P} (10 ⁻²² s s ⁻¹)	7.0(13)
Mass function, f (M_\odot)	0.1454196(33)
Orbital inclination (deg)	52
Total mass, M_{tot} (M_\odot)	2.4730(6) ^b
Pulsar mass, M_p (M_\odot)	1.25 ^{+0.06} _{-0.05}
Companion mass, M_c (M_\odot)	1.22 ^{+0.05} _{-0.06}
Angular distance from cluster center, θ_\perp (arcmin)	0.0784

Notes. Timing parameters and 1- σ uncertainties derived using TEMPO in Barycentric Dynamical Time (TDB), using the DE 430 Solar System ephemeris, the Terrestrial Time (BIPM) timescale and the DDFWHE orbital model.

^a Derived from $\dot{\omega}$ and γ and held fixed (see section 3.10). ^b Derived from $\dot{\omega}$.

d is the estimated distance to NGC 1851, its inverse is used for the parallax.

Estimate of v_T , \dot{P}_{int} and derived parameters assume d .

in time units, where c is the speed of light and G is Newton's gravitational constant.

value, $M_{\text{tot}} = 2.4730(6) M_\odot$ (see section 3.5). Thus, from eq. 1 we derive:

$$M_c = \frac{1}{\sin i} (f M_{\text{tot}}^2)^{\frac{1}{3}} = \frac{0.96166(16) M_\odot}{\sin i}, \quad (2)$$

this means that for the largest possible $\sin i$, M_c has a minimum value of 0.96166(16) M_\odot . The large mass for the companion and large eccentricity indicate that the system

The total mass M_{tot} was already presented by Freire et al. (2007), but in this work we present a much more precise

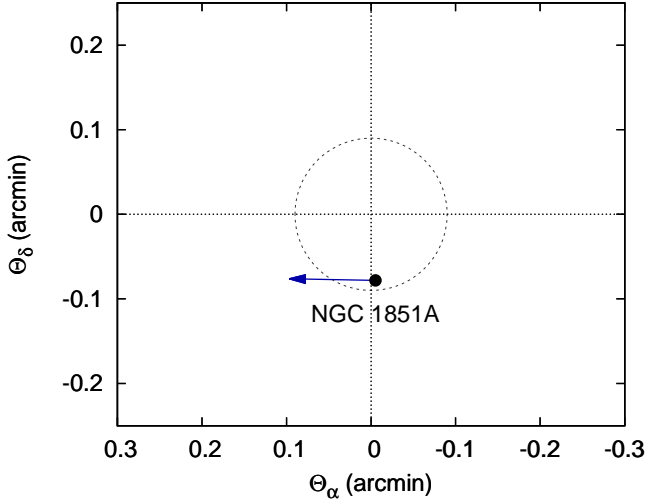


Figure 3. Position of NGC 1851A with respect to the nominal center of the cluster, located at $\alpha = 05^{\text{h}}14^{\text{m}}06.72^{\text{s}}$ and $\delta = -40^{\circ}02'44.2''$ (Gaia Collaboration et al. 2018). The dashed circle shows the core radius of NGC 1851, which is $0.09'$, according to Harris (1996, 2010 Edition). The blue arrow indicates the direction of the projected motion of the pulsar relative to the cluster.

is a product of a secondary exchange encounter, as already pointed out by Freire et al. (2007).

Knowing M_{tot} fixes the sum of the semi-major axes of both components of the binary, also known as the orbital separation, a , independently of the orbital inclination of the system. This results from Kepler's third law:

$$a = c \left[M_{\text{tot}} T_{\odot} \left(\frac{P_{\text{b}}}{2\pi} \right)^2 \right]^{1/3} = 2.79776(23) \times 10^{10} \text{ m}, \quad (3)$$

or $93.323(8)$ lt-s. We will need this value in some of the calculations below. This also implies that there is a minimum value of $\sin i$, which we can obtain from eq. 2 by assuming $M_p = 0$, $M_c = M_{\text{tot}}$; this is $\sin i > 0.3888$.

3.3 Variation of the spin period

The observed variation of the spin period is given by:

$$\left(\frac{\dot{P}}{P} \right)^{\text{obs}} = \left(\frac{\dot{P}}{P} \right)^{\text{int}} - \frac{\dot{D}}{D}, \quad (4)$$

where \dot{P}_{int} is the intrinsic spin-down of the pulsar and \dot{D} is the variation of the Doppler shift factor D . As already noticed by Freire et al. (2007), the observed \dot{P} is extremely small, our updated value is $7.0 \pm 1.3 \times 10^{-22} \text{ s s}^{-1}$, thus $(\dot{P}/P)^{\text{obs}} = 1.41(26) \times 10^{-19} \text{ s}^{-1}$.

The variation of the Doppler shift factor (D) consists of an acceleration term proportional to the distance, d and the square of the total proper motion, μ (Shklovskii 1970), another term due to the effect of the difference in the Galactic accelerations of the pulsar's system and the Solar System, projected along the direction from the pulsar to the Earth, a_l (Damour & Taylor 1991) plus, in this case, the (unknown)

acceleration of the system in the gravitational field of the cluster, a_g :

$$\frac{\dot{D}}{D} \equiv -\frac{\mu^2 d + a_l + a_g}{c}, \quad (5)$$

where, again, c is the speed of light. In order to separate it from the \dot{P}_{int} , Freire et al. (2017) used a similar expression for the orbital period:

$$\left(\frac{\dot{P}_{\text{b}}}{P_{\text{b}}} \right)^{\text{obs}} = \left(\frac{\dot{P}_{\text{b}}}{P_{\text{b}}} \right)^{\text{int}} - \frac{\dot{D}}{D}. \quad (6)$$

Subtracting equation (6) from equation (4) we obtain a result that does not depend on the acceleration or the proper motion of the system:

$$\Delta \equiv \left(\frac{\dot{P}}{P} \right)^{\text{obs}} - \left(\frac{\dot{P}_{\text{b}}}{P_{\text{b}}} \right)^{\text{obs}} = \left(\frac{\dot{P}}{P} \right)^{\text{int}} - \left(\frac{\dot{P}_{\text{b}}}{P_{\text{b}}} \right)^{\text{int}}. \quad (7)$$

Freire et al. (2017) then assumed that $\dot{P}_{\text{b}}^{\text{int}}$ is small to obtain estimates of the intrinsic \dot{P}^{int} for several MSPs in the globular cluster 47 Tucanae; these showed that they are very similar to the MSPs in the Galactic disk.

For NGC 1851A, we cannot make this assumption. The reason is that if we evaluate the left side of equation (7), we obtain $\Delta = -1.4(5) \times 10^{-17} \text{ s}^{-1}$. If $\dot{P}_{\text{b}}^{\text{int}}$ could be ignored, then Δ would be positive, since for a rotation-powered pulsar \dot{P}^{int} is always positive. The fact that it is negative means that it is possibly being compensated by a larger, positive $\dot{P}_{\text{b}}^{\text{int}}$. Because this analysis is independent of the system's acceleration, the negative Δ cannot be explained by the acceleration of the system in the gravitational field of a nearby star, or the cluster's. We discuss this in the following section.

Therefore, in order to estimate \dot{D}/D , we assume two extreme characteristic ages for the pulsar, 0.5 and 10 Gyr; these bracket the characteristic ages of most known MSPs. Using these ages, we get values for \dot{P}_{int} of $1.6 \times 10^{-19} \text{ s s}^{-1}$ and $7.9 \times 10^{-21} \text{ s s}^{-1}$ respectively. From equation (4), we then obtain for \dot{D}/D the extreme values of $3.2 \times 10^{-17} \text{ s}^{-1}$ and $1.44 \times 10^{-18} \text{ s}^{-1}$. After subtraction of the proper motion and Galactic acceleration terms, we obtain a very small line-of-sight acceleration for this binary system. This does not introduce any useful constraints on cluster mass models, for this reason we will not elaborate on it any further.

3.4 Variation of the orbital period

According to Lorimer & Kramer (2004), the observed variation of the orbital period is given by:

$$\begin{aligned} \left(\frac{\dot{P}_{\text{b}}}{P_{\text{b}}} \right)^{\text{int}} &= \left(\frac{\dot{P}_{\text{b}}}{P_{\text{b}}} \right)^{\text{obs}} + \frac{\dot{D}}{D} \\ &= \left(\frac{\dot{P}_{\text{b}}}{P_{\text{b}}} \right)^{\text{GW}} + \left(\frac{\dot{P}_{\text{b}}}{P_{\text{b}}} \right)^{\text{m}} + \left(\frac{\dot{P}_{\text{b}}}{P_{\text{b}}} \right)^{\text{T}}. \end{aligned} \quad (8)$$

Depending on the assumption above for $\dot{P}_{\text{b}}^{\text{int}}$ and \dot{D}/D we get for this sum a range of values from $1.6(5)$ to $4.5(5) \times 10^{-17} \text{ s}^{-1}$. This implies that the result appears to be at least $3\text{-}\sigma$ significant. However, we have noticed already that the value of $\dot{P}_{\text{b,obs}}$ has not fully stabilized yet. As shown in Fig. 4, as we add more and more epochs to our dataset, its positive value keeps changing and ultimately tends to decrease. For this reason, we will only present a brief discussion of this

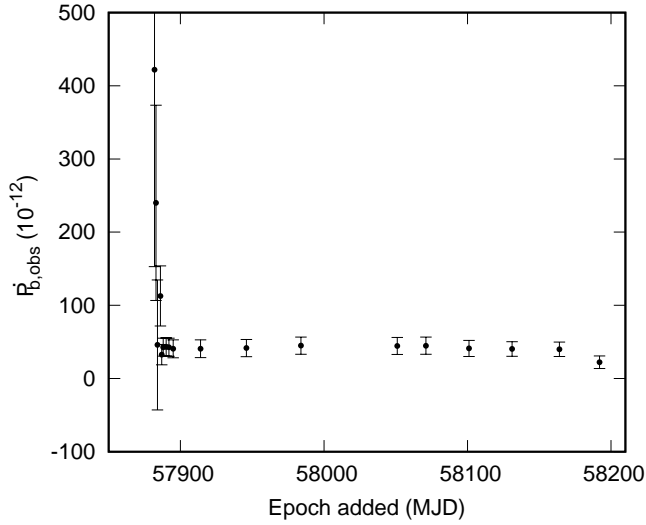


Figure 4. Orbital period derivative ($\dot{P}_{b,\text{obs}}$) of NGC 1851A measured using the DDFWHE binary model as a function of epoch added from uGMRT dataset (the GBT dataset is also always included in the fit). The last point, which is the one derived using the whole GBT+uGMRT dataset, is the value reported in Table 2.

effect below. In particular, we look at the individual terms and discuss whether they could yield a large, positive $\dot{P}_{b,\text{int}}$ or not.

The first term on the second line of equation (8) is due to loss of orbital energy caused by the emission of quadrupolar gravitational waves. Assuming the masses obtained in section 4, this is given in GR by (Peters 1964):

$$\dot{P}_{b,\text{GR}} = -\frac{192\pi}{5} T_{\odot}^{5/3} \left(\frac{P_b}{2\pi}\right)^{-5/3} f(e) \frac{M_p M_c}{M_{\text{tot}}^{1/3}} \quad (9)$$

$$f(e) = \frac{1}{(1-e^2)^{7/2}} \left(1 + \frac{73}{24}e^2 + \frac{37}{96}e^4\right). \quad (10)$$

For the masses of the system, as they are determined in section 4, we obtain $\dot{P}_{b,\text{GR}} = -0.155 \times 10^{-12} \text{ s s}^{-1}$, thus $\dot{P}_{b,\text{GR}}/P_b = -9.6 \times 10^{-20} \text{ s s}^{-1}$. This is two orders of magnitude smaller than Δ , thus it does not explain the anomalous Δ we observe.

The second term in the second line of equation (8) is caused by mass loss from the system. Assuming, as Damour & Taylor (1991) did, that this is dominated by the loss of rotational energy for the pulsar, this is given by :

$$\left(\frac{\dot{P}_b}{P_b}\right)^{\text{in}} = 2 \frac{\dot{m}}{M_{\text{tot}}} = 2 \frac{\dot{E}}{c^2 M_{\text{tot}}} \quad (11)$$

$$= \frac{8\pi G}{T_{\odot} c^5} \frac{I}{M_{\text{tot}}} \frac{\dot{P}_{\text{int}}}{P^3} \simeq 2.3 \times 10^{-4} \left(\frac{\dot{P}}{P}\right)^{\text{int}} \quad (12)$$

where $I \simeq 10^{38} \text{ kg m}^2$ is the moment of inertia of the pulsar. We can see from the last identity that this term is extremely small compared to \dot{P}_{int}/P , which is very similar to \dot{D}/D (equations 4 and 6). This means that this term cannot explain the observed Δ either.

However, if the companion is losing mass on its own at a sufficiently large rate, that could cause the observed Δ . Indeed, if we assume that Δ is caused by mass loss, we obtain:

$$\left(\frac{\dot{P}_b}{P_b}\right)^{\text{in}} \simeq \left(\frac{\dot{P}_b}{P_b}\right)^{\text{obs}} + \frac{\dot{D}}{D} > 1.55 \times 10^{-17} \text{ s}^{-1} \quad (13)$$

$$\dot{m} = \frac{M_{\text{tot}}}{2} \left(\frac{\dot{P}_b}{P_b}\right)^{\text{in}} \quad (14)$$

$$\dot{m} > 1.9 \times 10^{-17} M_{\odot} \text{ s}^{-1} = 6.1 \times 10^{-10} M_{\odot} \text{ yr}^{-1} \quad (15)$$

which is about 10^4 times larger than the current mass loss rate for the Sun. Such mass loss rates do not generally occur for compact objects (certainly not for NSs or heavy white dwarfs). However, as discussed by Freire et al. (2007), the lack of eclipses rules out extended companions, such as main sequence star companions, and even more a giant companion. Therefore, a large mass loss rate should not be expected.

Finally, the last term on the second line of equation (8) is caused by tidal dissipation. This might explain the observed Δ if the companion were extended and rotated fast and in the same sense of the orbit, as in the Earth-Moon system. However, since the companion does not appear to be extended, this is, again, an unlikely explanation.

Since the value of \dot{P}_b^{obs} has not fully stabilized yet, there is a chance that none of these effects (mass loss or tidal acceleration of the orbit) are real. To our knowledge, this effect has not been observed in any pulsars to date. Continued timing with the coherent de-dispersion mode will quickly improve its precision and robustness and confirm the increase in the orbital period or not.

3.5 Rate of advance of periastron

For NGC 1851A, the observed rate of advance of periastron, $\dot{\omega}_{\text{obs}}$ is measured very precisely: $\dot{\omega}_{\text{obs}} = 0.0129592(16) \text{ deg yr}^{-1}$. This is 25 times more precise and slightly larger than the value published by Freire et al. (2007), $\dot{\omega}_{\text{obs}} = 0.01289(4) \text{ deg yr}^{-1}$. As all measurements in this work, the latter's uncertainty is a 68.3 % confidence limit, equivalent to 1 σ in a normal distribution. Our new value is thus 1.7- σ larger than the earlier. This difference is not statistically significant.

According to Lorimer & Kramer (2004), in the absence of other massive objects near the binary, $\dot{\omega}_{\text{obs}}$ is given by:

$$\dot{\omega}_{\text{obs}} = \dot{\omega}_{\text{rel}} + \dot{\omega}_{\text{k}} + \dot{\omega}_{\text{SO}} \quad (16)$$

The first term is caused by relativistic effects. Assuming general relativity (GR), we can estimate the total mass of the binary, M_{tot} (in solar masses), from $\dot{\omega}_{\text{rel}}$ and the Keplerian parameters P_b and e (Robertson 1938) by inverting the well-known expression derived by Taylor & Weisberg (1982):

$$M_{\text{tot}} = \frac{1}{T_{\odot}} \left[\frac{\dot{\omega}_{\text{rel}}}{3} (1-e^2) \right]^{\frac{3}{2}} \left(\frac{P_b}{2\pi} \right)^{\frac{5}{2}}, \quad (17)$$

If $\dot{\omega}_{\text{rel}}$ fully accounts for $\dot{\omega}_{\text{obs}}$, then we can derive $M_{\text{tot}} = 2.47298(45) M_{\odot}$. This constraint is displayed by the red lines in figure 5.

However, $\dot{\omega}_{\text{rel}}$ does not fully account for the observations. The second term in equation (18), $\dot{\omega}_{\text{k}}$, is given by Kopeikin (1995), here re-arranged as in Freire et al. (2011b):

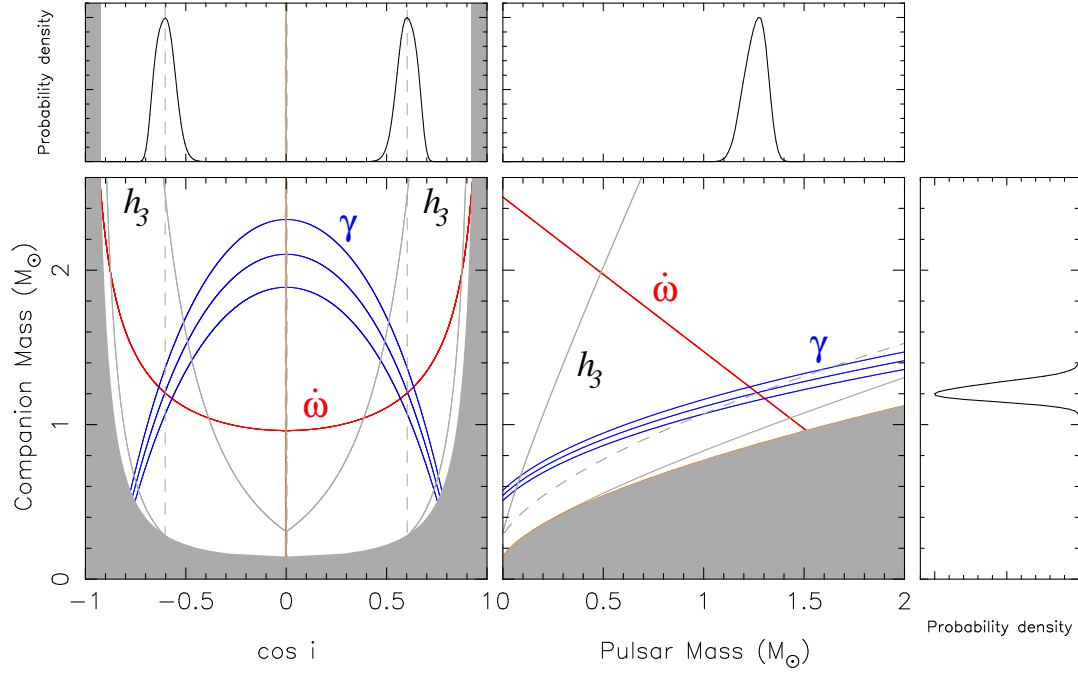


Figure 5. Mass constraints for PSR J0514–4002A. In the main square plots, the lines indicate the regions that are (according to general relativity) consistent with the nominal and $\pm 1\sigma$ measurements of $\dot{\omega}$ (solid red), γ (solid blue) and h_3 (gray) obtained from the DDFWHE model (see Table 2). For the h_3 estimate, we assumed the value of ζ marked by the dotted gray lines (section 3.10); only the nominal (near $M_p = 0$) and $+1\sigma$ lines are visible; the latter excludes orbital inclinations near 90 deg. In the left plot, we display $\cos i$ (for randomly inclined orbits this would have equal probability) versus the companion mass (M_c); the gray region is excluded by the mass function of the system - the pulsar mass (M_p) must be larger than 0. In the right plot, we display M_p versus M_c ; the gray region is excluded by the constraint $\sin i \leq 1$. The side panels display the 1-d pdfs for $\cos i$ (top left), M_p (top right) and M_c (right), normalized to the maximum (for details see section 4). The distribution for M_c is derived from the distribution for M_c using $M_p = M_{\text{tot}} - M_c$.

$$\dot{\omega}_k = \frac{\mu}{\sin i} \cos(\Theta_\mu - \Omega), \quad (18)$$

where Θ_μ is the position angle of the proper motion and Ω is the (unknown) position angle for the line of nodes. Maximizing this contribution, i.e., setting $\cos(\Theta_\mu - \Omega) = \pm 1$ (and using the value for $\sin i$, from section 3.6), we obtain $\dot{\omega}_k = \pm 1.82 \times 10^{-6} \text{ deg yr}^{-1}$, which is very similar to the measurement uncertainty. Thus the assumption that $\dot{\omega}_{\text{obs}}$ is caused by relativistic effects is mostly warranted, but $\dot{\omega}_K$ is already having an influence on the uncertainty of the measurement of the total mass of the binary.

The last term, $\dot{\omega}_{\text{SO}}$, has not yet been detected in any binary pulsar, so we will for now assume it does not contribute significantly.

As we will see in section 4, we have at the moment no way of measuring Ω . Therefore, $\dot{\omega}_k$ cannot be evaluated, beyond the lower and upper limits we have estimated. This means that the uncertainty of M_{tot} has to be increased to take into account the unknown contribution of $\dot{\omega}_k$. Adding the maximum value of $\dot{\omega}_k$ to the uncertainty of $\dot{\omega}_{\text{obs}}$, we obtain an estimate for the uncertainty of the latter: $2.4 \times 10^{-6} \text{ deg yr}^{-1}$. This translates into a M_{tot} uncertainty of $6 \times 10^{-4} M_\odot$, which is the uncertainty quoted in Table 2.

3.6 Einstein delay

The main new result in this paper is the measurement of the Einstein delay, γ . This measures the apparent slowdown of

the rotation of the pulsar near periastron relative to apastron. Assuming that it is solely an effect of GR (an assumption we discuss in detail below), 50% of the effect is caused by the varying special-relativistic time dilation (which is caused by the varying velocity of the pulsar in its orbit) and 50% by the varying gravitational redshift.

Until now, this has been measured only for eccentric systems with orbital periods of 10 hr (for PSR B15134+12, see Fonseca et al. 2014) or shorter, all of these being double neutron star systems. The orbital period of NGC 1851A is 45 times larger than that of PSR B15134+12. This detection was helped by the magnitude of the effect, $\gamma = 21.6(9) \text{ ms}$; by far the largest ever measured in any binary pulsar.

In GR, this effect is related to the component masses by the equation

$$\gamma = \gamma_K \frac{M_c(M_c + M_{\text{tot}})}{M_{\text{tot}}^{4/3}} \quad (19)$$

$$\gamma_K = T_\odot^{2/3} e \left(\frac{P_b}{2\pi} \right)^{1/3}, \quad (20)$$

these constraints are depicted by the blue lines in Fig. (5). The reason for the large γ of PSR J0514–4002A has to do with the γ_K term being larger for this pulsar, a consequence of the large values for e and P_b .

If we already know M_{tot} , we can determine the masses

from γ using

$$M_c = \frac{1}{2} \left(\sqrt{M_{\text{tot}}^2 + 4M_{\text{tot}}^{4/3} \frac{\gamma}{\gamma_K}} - M_{\text{tot}} \right) \quad (21)$$

$$M_p = M_{\text{tot}} - M_c; \quad (22)$$

for the γ and M_{tot} measured for PSR J0514–4002A, the result is $M_c = 1.207_{-0.038}^{+0.037} M_\odot$ and $M_p = 1.266_{-0.037}^{+0.038} M_\odot$, assuming GR.

Inverting equation (2) we obtain $\sin i = 0.797$, which implies either $i = 53.8$ deg or $i = 127.2$ deg. These values are represented by the intersection of the red and blue lines in Fig. 5.

3.7 Covariance of the Einstein delay with \dot{x} for wide orbits

We now examine the assumption that the observed γ is solely an effect of GR. We start by examining why measurements of γ for wide binary pulsars have not been made to date, despite the (often) very large expected values of γ_K and in some cases M_c as well.

As pointed out by Blandford & Teukolsky (1976), and later more explicitly by Wex et al. (1998), we cannot measure γ for a single orbit (even if measured with extreme precision) because the effect is re-absorbed into the Keplerian parameters x and ω . If x and ω are the “real” projected semi-major axis and longitude of periastron for a particular binary, the measurable, “post-absorption” quantities x' and ω' are given, to very good approximation, by (Wex et al. 1998):

$$x' = x + \frac{\gamma}{\sqrt{1-e^2}} \cos \omega \quad (23)$$

$$\omega' = \omega - \frac{\gamma}{x\sqrt{1-e^2}} \sin \omega, \quad (24)$$

for the parameters of NGC 1851A, we get $x' = 36.29656$ lt-s and $\omega' = 82.2665$ deg, a difference of $0.00627(26)$ lt-s and $-0.0737(30)$ deg relative to the x and ω in Table 2. The uncertainties of the differences are calculated from the uncertainty of γ .

In order to measure γ , we must in effect measure x' for sufficiently spaced values of ω . Given the large $\dot{\omega}$ for the most compact and eccentric double neutron star systems, such a measurement is generally achievable for timing baselines of a few years. In the case of NGC 1851A, the $\dot{\omega}$ is only $0.0129592(16)$ deg yr $^{-1}$, which means that a full precession cycle lasts $27,779 \pm 3$ years. This is, of course, much longer than the timing baseline for this system, implying that we can only observe the system at closely spaced values of ω .

In such cases, we can only measure the current derivative of x' . Differentiating the last equations we obtain:

$$\dot{x}' = \dot{x} - \frac{\gamma \dot{\omega}}{\sqrt{1-e^2}} \sin \omega \quad (25)$$

$$\dot{\omega}' = \dot{\omega} - \frac{\gamma \dot{x}}{x^2 \sqrt{1-e^2}} \cos \omega + \frac{\gamma \dot{\omega}}{x \sqrt{1-e^2}} \sin \omega, \quad (26)$$

where we assumed that e and γ are constant.

Assuming specifically the DD model, we find that in the equations above e should be replaced by e_θ , which is given by:

$$e_\theta = e(1 + \delta_\theta), \quad (27)$$

where δ_θ is a PK parameter, the relativistic deformation parameter. In GR, this is expected to be 3.78×10^{-7} for NGC 1851A. This parameter is not separately measurable for this pulsar. The difference between e and e_θ is so small that it can be ignored in the discussion that follows.

The difference between $\dot{\omega}$ and $\dot{\omega}'$, 2.24×10^{-6} deg yr $^{-1}$, is similar to the uncertainty on $\dot{\omega}$, for that reason we will also ignore it for the time being (it is taken into account anyway when we fit for γ).

Since we only really measure \dot{x}' , we cannot separate the intrinsic variation of the projected semi-major axis (\dot{x}) from γ , both quantities are completely covariant (eq. 25). Indeed, if we fit for both quantities in TEMPO, we cannot determine either with any useful precision.

Since we have only fitted for γ in our timing solution (not for \dot{x}), the \dot{x}' should be given by the γ term in equation (25):

$$\dot{x}' = -3.34(14) \times 10^{-13} \text{ lt-s s}^{-1}, \quad (28)$$

where the uncertainty is derived from the uncertainty of γ .

We can test these expressions very easily by fitting the DDFWHE solution with \dot{x} instead of γ . Doing this we obtain a fit with basically the same χ^2 (927.29) and the following parameters:

$$x = 36.29658(6) \text{ lt-s}, \quad (29)$$

$$\omega = 82.266526(31) \text{ deg}, \quad (30)$$

$$\dot{x} = -3.34(14) \times 10^{-13} \text{ lt-s s}^{-1}, \quad (31)$$

which agree within $1-\sigma$, and exactly with our expectation for the “absorbed” values x' , ω' and \dot{x}' respectively.

If the intrinsic \dot{x} is small compared to \dot{x}' in equation (25) (or if it can be determined independently with a precision that is small compared to \dot{x}'), then we can measure γ and use it to determine the masses. If not, then it becomes impossible to measure γ and determine reliable masses from it. This is a general condition that must be evaluated before attempting to determine γ for any wide binary system. We estimate \dot{x} in the next section.

However, before we proceed, we remark that equation (25) implies that, for some wide binaries (those with ω close to 0 deg or 180 deg) the $\sin \omega = 0$ term makes it virtually impossible to measure γ for those binaries, at least while that ω configuration persists (which can be many thousands of years). One of the factors that allows the measurement of γ for NGC 1851A is the favourable ω of 82.34 deg, which almost maximizes the possible contribution of γ to \dot{x}' .

3.8 Variation of the projected semi-major axis

Since we have no independent way of measuring \dot{x} , it is very important to carefully estimate it. We do this in this section within the framework of GR.

According to Lorimer & Kramer (2004), the change in \dot{x} can be written, in the absence of any massive objects in the vicinity of the binary, as:

$$\left(\frac{\dot{x}}{x} \right) = \left(\frac{\dot{x}}{x} \right)^k + \left(\frac{\dot{x}}{x} \right)^{\text{GW}} + \frac{d\epsilon_A}{dt} - \frac{\dot{D}}{D} + \left(\frac{\dot{x}}{x} \right)^m + \left(\frac{\dot{x}}{x} \right)^{\text{SO}} \quad (32)$$

The first term is caused by the changing geometry due to the motion of the system relative to the Earth and it is given

by (Kopeikin 1995):

$$\left(\frac{\dot{x}}{x}\right)^k = \mu \cot i \sin(\Theta_\mu - \Omega), \quad (33)$$

where we have, again, re-written the terms as in Freire et al. (2011b), except for the latter's negative sign; the reason for this is that the system we use to measure Ω and i should be a right-handed system. Using the most likely value of $\sin i$ from section 3.6, we obtain for this term a maximum and minimum values (corresponding to $\sin(\Theta_\mu - \Omega) = \pm 1$) of $\pm 6.05 \times 10^{-16} \text{ s}^{-1}$. This implies $\dot{x}_k = \pm 2.2 \times 10^{-14} \text{ lt-s s}^{-1}$. This is about 6.5% of \dot{x}' . Therefore, any computation of the component masses will have to take this effect into account.

The second term is from the decrease of the size of the orbit caused by gravitational wave emission; this is given by

$$\left(\frac{\dot{x}}{x}\right)^{\text{GW}} = \frac{2}{3} \frac{\dot{P}_{\text{b,GW}}}{P_{\text{b}}} = -6.4 \times 10^{-20} \text{ s}^{-1}, \quad (34)$$

i.e., $\dot{x}_{\text{GW}} = -2.3 \times 10^{-18} \text{ lt-s s}^{-1}$. This is four orders of magnitude smaller than \dot{x}_k .

The third term, caused by aberration, is proportional to the geodetic precession rate for the pulsar. This is given by Barker & O'Connell (1975) as:

$$\Omega_{\text{geod}} = \left(\frac{2\pi}{P_{\text{b}}}\right)^{5/3} T_{\odot}^{2/3} \frac{1}{1-e^2} \frac{M_c(4M_{\text{tot}} - M_c)}{2M_{\text{tot}}^4/3}, \quad (35)$$

assuming the mass values derived in section 4 and the Keplerian parameters of the system, we obtain $\Omega_{\text{geod}} = 0.0037 \text{ deg yr}^{-1}$. The aberration term is proportional to the latter (Damour & Taylor 1992):

$$\frac{d\epsilon_A}{dt} = \frac{P}{P_{\text{b}}} \frac{\Omega_{\text{geod}}}{\sqrt{1-e^2}} \frac{\cot \lambda \sin 2\eta + \cot i \cos \eta}{\sin \lambda}, \quad (36)$$

where η and λ are the polar coordinates of the pulsar's spin. For NGC 1851A the non-geometric factors (the first two fractions in the equation above) amount to $1.37 \times 10^{-20} \text{ s}^{-1}$, i.e., the variation of x caused by this term is about $5.0 \times 10^{-19} \text{ lt-s s}^{-1}$. This is more than four orders of magnitude smaller than \dot{x}_k .

The fourth term is caused by the variation of the Doppler shift. From the assumption in section 3.4 of a characteristic age larger than 0.5 Gyr, it was deduced that $\dot{D}/D < 3.2 \times 10^{-17} \text{ s}^{-1}$, i.e., its contribution to \dot{x} is $-1.1 \times 10^{-15} \text{ lt-s s}^{-1}$. This is one order of magnitude smaller than \dot{x}_k .

The fifth term can be derived from \dot{P}_{b}^m being given by equation (13). If we use in that equation the upper estimate of \dot{D}/D , as discussed in section 3.3, then we get $(\dot{P}_{\text{b}}/P_{\text{b}})^m < 4.6 \times 10^{-17} \text{ s s}^{-1}$. Using equation (34), we obtain $(\dot{x}/x)^m = 3.04 \times 10^{-17} \text{ s}^{-1}$, i.e., $\dot{x}_m = 1.1 \times 10^{-15} \text{ lt-s s}^{-1}$. This is one order of magnitude smaller than \dot{x}_k , furthermore, it is of a sign opposite to that of the contribution from \dot{D}/D and of very similar magnitude.

The sixth and last term, \dot{x}^{SO} , has two contributions: the relativistic spin-orbit coupling, also known as the Lense-Thirring effect (\dot{x}_{LT}), caused by the rotation of the pulsar or the companion, and the classical spin-orbit coupling (\dot{x}_{QM}). Generally, for main sequence stars \dot{x}_{QM} is much larger than \dot{x}_{LT} , for NSs the opposite is true, and for white dwarfs (WDs) both terms are roughly similar.

For the Lense-Thirring effect, we have (Damour & Taylor 1992):

$$\dot{x}_{\text{LT}} \simeq -x \frac{G S_A}{c^2 a^3 (1-e^2)^{3/2}} \left(2 + \frac{3M_B}{2M_A}\right) \cot i \sin \delta_A \sin \Phi_A^0 \quad (37)$$

where $S_A = I_A \Omega_A$ is the rotational angular momentum of component A, I_A is that component's moment of inertia and Ω_A is that component's angular frequency, δ_A and Φ_A^0 are angles that determine the alignment of the rotation of component A relative to the orbit and a is the orbital separation calculated in equation (3).

We now evaluate this term for the pulsar. For NSs, the moment of inertia is generally assumed to be of the order of 10^{38} kg m^2 . For the pulsar, the angular frequency is well known, $\Omega_{\text{p}} = 2\pi/P = 1259.01 \text{ rad s}^{-1}$, thus $S_{\text{p}} \sim 1.25 \times 10^{41} \text{ kg m}^2 \text{ s}^{-1}$. Therefore,

$$\dot{x}_{\text{LT}} \simeq -3 \times 10^{-15} \sin \delta_{\text{p}} \sin \Phi_{\text{p}}^0 \text{ lts s}^{-1}, \quad (38)$$

which is one order of magnitude smaller than the kinematic term \dot{x}_{K} . This will therefore have no impact on the mass measurements.

If the companion is a NS, then the same calculation can be made, except for the lack of knowledge of the spin period. The contribution to \dot{x} is only similar to \dot{x}_{K} if the spin period is of the order of 0.5 ms, a rotational velocity ~ 3 times faster than any pulsar observed to date. This is unlikely.

Not much changes if the companion is a WD: we still do not know its rotational angular momentum, S . The moment of inertia for a massive WD is about 10^4 times larger than for a NS. The shortest spin period known for a WD is 13.2 s (Mereghetti et al. 2009). Thus, if the companion to NGC 1851A were spinning at 13.2 s, the total angular momentum would be $S_{\text{p}} \sim 4.8 \times 10^{41} \text{ kg m}^2 \text{ s}^{-1}$, and

$$\dot{x}_{\text{LT}} \sim -1.1 \times 10^{-14} \sin \delta_{\text{C}} \sin \Phi_{\text{C}}^0 \text{ lts s}^{-1}, \quad (39)$$

which would be of the order of half of the estimated \dot{x}_{K} .

Finally, if the companion is a WD, there will be a contribution of the classical spin-orbit coupling to \dot{x} , caused by the rotationally-induced oblateness of the companion. This is given by Wex et al. (1998):

$$\dot{x}_{\text{QM}} = x \left(\frac{2\pi}{P_{\text{b}}}\right) Q \cot i \sin \delta_{\text{c}} \cos \delta_{\text{C}} \sin \Phi_{\text{C}}^0 \quad (40)$$

where:

$$Q = \frac{k_2 R_{\text{C}}^2 \hat{\Omega}_{\text{C}}^2}{a^2 (1-e^2)^2} \quad \text{with} \quad \hat{\Omega}_{\text{C}} \equiv \frac{\Omega_{\text{C}}}{(Gm_{\text{C}}/R_{\text{C}}^3)^{1/2}}, \quad (41)$$

where $m_{\text{C}} = 2.4 \times 10^{30} \text{ kg}$ is the companion mass in kg, R_{C} is its radius ($\sim 3000 \text{ km}$), and k_2 is its apsidal motion constant, which is a dimensionless measure of the oblateness of the companion; for WDs this is of the order of 0.1 (Boshkayev et al. 2017). For a spin period of 13.2 s, we have $\hat{\Omega} \sim 0.2$, thus $Q \sim 7.8 \times 10^{-10}$ and

$$\dot{x}_{\text{QM}} \sim 8 \times 10^{-14} \sin \delta_{\text{c}} \cos \delta_{\text{C}} \sin \Phi_{\text{C}}^0 \text{ lts s}^{-1}, \quad (42)$$

which, depending on the angles, could be few times larger than \dot{x}_{K} and is comparable in magnitude with \dot{x}' .

Although this is unlikely, we cannot exclude the possibility of a fast-rotating WD companion. If we have a large contribution of \dot{x}_{LT} and \dot{x}_{QM} to \dot{x} , we have no way of separating it from the other effects.

3.9 Influence of the proper motion on the Einstein delay

As we have seen in the previous section, unless the companion is a WD with a very fast rotation, \dot{x}_k is by far the dominant contribution to \dot{x} , amounting up to $\pm 6.5\%$ of \dot{x}' . We will from now on assume that this is, indeed, the case.

Inverting equation (25), and using equation (18), we obtain the variation of the actual γ as a function of the proper motion μ , Ω , i and the measured γ for systems like NGC 1851A:

$$\gamma(\Omega, i) = \gamma + \frac{x\sqrt{1-e^2}}{\sin\omega} \frac{\mu}{\dot{\omega}} \cot i \sin(\Theta_\mu - \Omega), \quad (43)$$

from this we obtain maximum and minimum values of $\gamma(\Omega, i)$ of 23.1 and 20.3 ms respectively (the “measured” value, γ , is 21.6 ms) for values of i close to the values derived in section 3.6. These differences are slightly larger than the uncertainty of the measured γ , which is about 0.9 ms. Using equation (21), we can then obtain maximum and minimum companion masses of 1.263 and 1.144 M_\odot ; again these differences (of the order of 0.06 M_\odot) are larger than the mass uncertainties derived in section 3.6 from the uncertainty of the measured γ , 0.038 M_\odot .

We note that these estimates rely on our current measurement of the proper motion which, for the reasons discussed in section 3.1) is not yet fully trustworthy. If it is closer to the smaller GAIA proper motion of NGC 1851, then we would also have a smaller mass uncertainty caused by the proper motion.

3.10 Shapiro delay

The far from edge-on inclination means that the Shapiro delay is not easy to measure. In order to quantify its detectability we use the orthometric parameterization of Freire & Wex (2010), which is implemented as the DDFWHE model. To do this, we need first a numerical value for the orthometric ratio ς , this can be derived from the $s \equiv \sin i$ estimated in section 3.6:

$$\varsigma = \frac{s}{1 + \sqrt{1-s^2}} \simeq 0.50 \quad (44)$$

Fixing this in the model, we fit the orthometric amplitude, obtaining $h_3 = 0.2 \pm 1.4 \mu\text{s}$. This means that the Shapiro delay is not detectable in this system. However, this value of h_3 is 1- σ consistent with the expectation for this system, $h_3 = M_c T_\odot \varsigma^3 \simeq 0.74 \mu\text{s}$.

Despite being a non-detection, this constraint can already exclude inclinations close to edge-on, as seen in figure 5.

4 BAYESIAN ANALYSIS OF THE COMPONENT MASSES

In order to estimate the influence of the proper motion on γ , we used in the previous section a value of $\cot i$ that is itself derived from the mass function of the system and the component masses. The problem is that the component masses must be derived from $\gamma(\Omega, i)$ itself.

For this reason, we have implemented a Bayesian analysis of the system, with the aim of determining the masses and

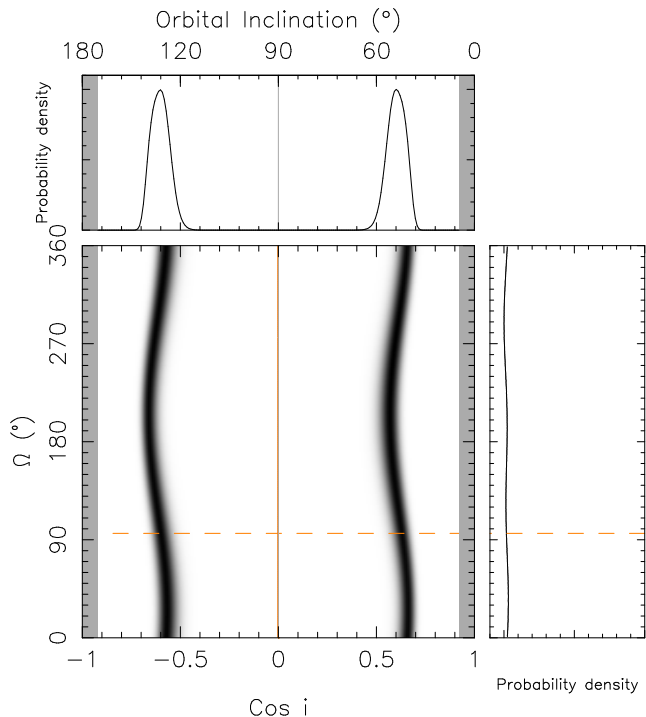


Figure 6. *Central panel:* the full $\cos i$ - Ω space for binary pulsars. For PSR J0514–4002A, the gray regions are excluded by the requirement that the pulsar mass must be larger than 0. The dotted orange line indicates the position angle of the proper motion of the system. The grey scale indicates the probability density, with zero indicated by white and maximum probability density indicated by black. As we can see, the best orbital inclination varies significantly with Ω . *Top panel:* probability density function for $\cos i$, normalized to the maximum. *Right panel:* probability density function for Ω . This is almost uniform, i.e., this variable is not constrained for this system.

orbital inclinations of the system in a fully self-consistent manner.

4.1 Mapping the orbital orientation space

In what follows, we roughly follow the Bayesian analysis done by Stovall et al. (2018a), but with a few important differences. As in the latter work, we map the quality of fit (the residual χ^2) for the orbital orientation space ($\cos i$ and Ω) using the DDK orbital solution. The full space ranges from $\cos i = -1$ to 1 and from $\Omega = 0$ deg to 360 deg. Randomly oriented orbits will populate this space uniformly. In practice, we limit the range of i to regions where M_p is positive, i.e., where $\sin i > 0.3888$. Thus $-0.9213 < \cos i < 0.9213$.

Unlike Stovall et al. (2018a), we do not sample the third dimension (in the latter case M_{tot}) because, as discussed in section 3.5, the changes in the total mass caused by the kinematic contribution $\dot{\omega}_k$ are of the same order of the measurement uncertainty for $\dot{\omega}$. The resulting changes in M_{tot} with Ω are two orders of magnitude smaller than the uncertainties in the masses of the components; therefore they are irrelevant for the estimates of the component masses. For

this reason, the whole map assumes one value of M_{tot} for the estimation of the component masses.

For each point in the grid of $\cos i$ and Ω values, we introduce these values in the DDK model via the TEMPO's KIN and KOM parameters. From this, the model internally estimates all kinematic effects, particularly the secular \dot{x} .

For each value of i , we derive M_c from equation (2). We then introduce it in the model via the TEMPO's M2 parameter. This completes the description of the Shapiro delay: its first parameter is the orbital inclination i .

Then, for each point we estimate γ from M_c and M_{tot} using equation (19), we introduce the result in the model via TEMPO's GAMMA parameter.

All these parameters (i , Ω , M_c and γ) are fixed inputs to the DDK model used to do the timing analysis for that grid point. We then run TEMPO, fitting for all other relevant timing parameters, including $\dot{\omega}$, which is allowed to oscillate a little around the best-fit model because of $\dot{\omega}_K$, and \dot{P}_b , which is dominated by kinematic effects. We then record the value of the χ^2 for each combination of Ω and $\cos i$. The resulting 2-D grid of χ^2 values are then used to calculate a 2-dimensional probability density function (pdf) for Ω , $\cos i$, as discussed by Splaver et al. (2002):

$$p(\Omega, \cos i) \propto e^{-\frac{\chi^2_{\text{min}} - \chi^2}{2}}, \quad (45)$$

where χ^2_{min} is the lowest χ^2 of the whole grid. A greyscale plot of this pdf is displayed in the central plot of Fig. 6.

This 2-D pdf is then projected along two axes, $\cos i$ (1-D pdf is shown on top left panel in Fig. 5 and top panel in Fig. 6) and Ω (1-D pdf in right panel of Fig. 6). This is then translated into the M_c axis using equation (2) (1-D pdf in right panel of Fig. 5). The 1-D pdf for M_p (top right panel of Fig. 5) is merely a reflection of the pdf for M_c .

4.2 Results

In Fig. 6, we can see how the orbital inclination derived from $\dot{\omega}$ and γ varies as a function of Ω , this is a visual demonstration of the effect of the proper motion on γ . These orbital inclinations have identical probabilities because the Shapiro delay is not measured with enough precision to further restrict $\cos i$. One of the consequences of this is that, as we can see on the right plot, the probability density function for Ω is nearly constant.

The derived pulsar mass is $1.25_{-0.06}^{+0.05} M_{\odot}$ to 68.3 % confidence limit (C.L.) and $1.25_{-0.12}^{+0.09} M_{\odot}$ to 95.4 % C.L.; the asymmetry of the pdf can be easily be seen in Fig. 5. This mass is slightly lower, but consistent, with the simple estimate made in section 3.6. For the companion mass, the distribution is inverted: $M_c = 1.22_{-0.05}^{+0.06} M_{\odot}$ to 68.3 % C.L. and $1.22_{-0.09}^{+0.12} M_{\odot}$ to 95.4 % C.L.

The mass of NGC 1851A is one of the lowest MSP masses measured to date. There is only one other MSP, PSR J1918–0642 ($M_p = 1.29_{-0.09}^{+0.10} M_{\odot}$ Arzoumanian et al. 2018) that could have such a low mass. This measurement demonstrates that the recycling to a spin period of ~ 5 ms can be achieved with a small amount of mass: even if the system formed with the lowest known NS mass, $1.174(4) M_{\odot}$ (Martinez et al. 2015), the recycling process would have been accomplished with a mass transfer of $\sim 0.08 M_{\odot}$.

On the other hand, the mass we measured for the com-

panion implies that it can be also a NS. We will explore this possibility in the following section.

5 COMPANION SEARCH

If the companion is a NS, it could in principle also be a radio pulsar. For this reason, we carried out a search for pulsations from the putative companion.

For each observation listed in Table 1 (taking the CDP data whenever available, PA data otherwise) we first created a mask with the `rfifind` routine of PRESTO, in order to exclude all those frequency channels and time intervals affected by RFI. Taking the masks into account, we then used the `prepdata` routine to de-disperse all the data at the nominal DM of NGC 1851A (52.14 pc cm^{-3}), scrunch the frequency band and create a *barycentered* (i.e. referred to the SSB) time series for each observation. In doing so, the CDP observations were also downsampled by a factor of eight, in order to match the sampling time of the PA data.

The actual search for the radio pulsations was done as follows. First, we used the PYSOLATOR⁹ software package to remove the orbital motion of the putative companion pulsar. In essence, PYSOLATOR subtracts the predicted orbital Rømer delay, together with any other relativistic effects, from each sample of the time series. As a result, it outputs a new demodulated time series, where the pulsar appears as if it were isolated and located at the binary barycentre. By subtracting the orbital motion, the observed spin period of the possible companion pulsar will appear constant within each observation, as well as across multiple observations¹⁰. This means that there is no need to perform an acceleration search, and our sensitivity will not be limited by the length of the single observation (Ransom 2001). All of this is possible only if we have good knowledge of the system's mass ratio, $q = M_p/M_c$. This is because we know all the characteristics of the companion's orbit very precisely, with the exception of its projected semi-major axis, x_c . The latter is related to the projected semi-major axis of the pulsar orbit, x_p , as $x_c = q x_p$. Given the uncertainties on M_p and M_c , the mass ratio is in the range $q = 0.929 - 1.111$ to 68.3% C.L., therefore it is a parameter of our search.

Therefore, we tried several values of q and, for each of them, all the demodulated time series were Fourier transformed with the `realfft` routine of PRESTO. The so produced power spectra, after being de-reddened and normalized with PRESTO's `rednoise`, were summed together to produce a single stacked power spectrum relative to each considered trial q value. In order to properly sum the spectra together, each demodulated time series was padded by PYSOLATOR so as to artificially obtain all time series with the same number of samples as that of the longest observation. To avoid sudden jumps in the time domain, which would translate into artifacts in the Fourier domain, the added samples were all set to the average value of the last 10% of the original time series. This approach, which was also recently used by, e.g.,

⁹ <https://github.com/alex88ridolfi/pysolator>

¹⁰ This is strictly true only if we ignore the intrinsic spin-down of the pulsar. Given the small time span of our dataset, this is a safe assumption.

Cadelano et al. (2018), allowed us to retain phase coherence within each observation and at the same time to have the resulting power spectra with homogeneous characteristics (i.e. Fourier bin size and frequency span), thus being straightforward to sum together.

Clearly, the range of q values had to be explored with a sensible choice of the step size, Δq . The latter was chosen by imposing that, in the case of the best trial value and the fastest possible companion pulsar considered (i.e. spinning at 1000 Hz), the *maximum* drift of the observed spin frequency in the Fourier domain would be smaller than the size of one Fourier bin. For our dataset, this resulted in $\Delta q = 0.00018$, corresponding to a total of 1011 trial values of q . The so obtained 1011 stacked spectra were then searched with PRESTO's `accelsearch`, allowing no acceleration. All the candidates were then sifted, removing duplicates and excluding those with a significance of $\sigma < 5.0$. The candidates that survived the selection criteria were then folded using the original search-mode data, so as to retain full frequency information. This was done by producing, for each candidate, an ad-hoc ephemeris of the putative companion, containing the candidate spin frequency, as well as the orbital parameters as derived from the considered q value. The resulting diagnostic plots were then inspected by eye.

None of the candidates could be ascribed to an astrophysical pulsar-like signal.

6 DISCUSSION AND CONCLUSIONS

6.1 On the nature of the companion

The mass measurements for this system make it comparable to the highly eccentric PSR J1807–2500B in NGC 6544 (Lynch et al. 2012), where the companion, with a mass of $1.2064(20) M_{\odot}$, might also be a NS. The companions to these systems could also be massive WDs.

There are systems in the Galactic disk with similar eccentricities, the double neutron star systems (DNSs). One of them, PSR J1811–1736, even has an orbital period and orbital eccentricity similar to NGC 1851A (Corongiu et al. 2007). However, it is unlikely that NGC 1851A formed like a DNS: all pulsars in DNSs have much longer spin periods than NGC 1851A (the shortest is that of PSR J1946+2052, 16.7 ms, Stovall et al. 2018b, PSR J1811–1736 itself has a spin period of 104 ms); this is a consequence of the fast evolution of the massive companion, which results in a relatively short accretion episode and therefore not much time for spin-up.

From this we conclude that systems like PSR J1807–2500B and NGC 1851A formed in a secondary exchange encounter, a likely event in the core of dense clusters like NGC 1851 and NGC 6544. Such encounters happen (by definition) after the pulsar was recycled by accretion of mass and angular momentum from a lighter companion, which can last long enough to spin up the pulsar significantly. During the encounter, a massive degenerate object came to such a close distance to the earlier binary system that a chaotic interaction ensued. In this case, the most likely result is the ejection of the lighter component of the binary and the formation of a new more compact and eccentric binary consisting of the pulsar and the massive degenerate intruder.

A consequence of the exchange interaction is that we cannot use stellar evolution arguments to clarify the nature of the companion of NGC 1851A. Given the possibility that the latter is a NS, we have made a deep search for radio pulsations from that companion, as described in section 5. No pulsations were found. This means that the question of the nature of the companion remains open: indeed, the non-detection of the companion is not conclusive since many NS companions to DNS systems are not detectable as pulsars either; the same is true for the vast majority of NSs in our Galaxy and in GCs.

It is highly unlikely that the companion is a main sequence star. Superior conjunction happens about 5 minutes after periastron, and the separation between the pulsar and its companion in the plane of the sky is scarcely more than one solar radius (Freire et al. 2007); a main-sequence companion would almost certainly produce eclipses near superior conjunction, which are not observed.

6.2 Is the companion losing mass?

The apparent detection of an intrinsic increase of the orbital period is intriguing. As calculated in section 3.4, if this is caused by mass loss from the companion, then it is losing mass at a rate that is about 10^4 times larger than the current mass loss rate for the Sun.

This is interesting because Freire et al. (2007) presented some evidence (based on the scintillation timescale of the pulsar, which seems to be inversely proportional to the orbital velocity of the pulsar around the centre of mass of the system) of some mass loss from the companion. Another possibility is that the \dot{P}_b^{int} has a tidal origin, with rotational energy of the companion being transferred to the orbit (thus increasing the period).

In either case, a confirmation of the large \dot{P}_b^{int} would imply that the companion is not a NS, because a NS companion would not likely lose mass at any appreciable rate (owing to its extreme gravity) or have a tidal interaction with the pulsar. We are thus left with the possibility of a massive WD companion. If this is losing mass, it must be at its late stages of formation, where the last vestiges of its envelope are still being ejected, otherwise no tidal effects are possible. We find that such a hypothesis is unlikely: any progenitors of $1.22 M_{\odot}$ WDs should have long disappeared from the stellar population of NGC 1851. In any case, optical observations of the companion to NGC 1851A are strongly encouraged.

6.3 Continued timing

Apart from the issue of the \dot{P}_b , there is another unsolved issue remaining, the proper motion. This is very different than the proper motion of the cluster and would suggest the pulsar is on an escape path. The other is the large and unexpected \dot{P}_b for this system. Both issues could arise from the 10-year gap in timing, where the phase evolution of the pulsar has not been measured. Continued timing should allow a better measurement of the higher spin frequency derivatives, the proper motion and \dot{P}_b , potentially allowing a full reconstruction of the spin evolution during the 10-year gap in observations. These measurements will certainly help clarify the issues raised by their current values.

Continued timing with the CDP mode will also improve the measurement of γ ; its uncertainty scales with $T^{-3/2}$, where T is the timing baseline. This will result in much thinner black lines in Fig. 6, i.e, a much more restricted range of Ω and $\cos i$ where the system might exist.

Furthermore, a few long observing sessions around periastron in CDP mode will certainly improve the constraints on the orthometric amplitude of the Shapiro delay, h_3 . This could in principle allow a measurement of the masses that is independent of γ and any possible contributions to \dot{x} that it might have. Restricting the range of inclinations would imply (as we can see looking at Fig. 6) a restriction of the possible values of Ω .

6.4 Conclusions

In this paper, we have presented the results for the recent timing of the NGC 1851A binary pulsar with the uGMRT. Combining our ToAs with those obtained with GBT 10 years before, we greatly improve the precision of the measurement of $\dot{\omega}$, thus obtaining a far more precise estimate of the total mass of the binary. We also measure, for the first time, the proper motion of the system and the relativistic Einstein delay, γ . This is the first time this has been done for a system with an orbital period larger than 10 hours. The detection is helped by the sheer magnitude of the effect, which is 4.5 times larger than any measurement of γ made to date in a binary pulsar. This is also the first time that a measured γ is larger (in this case four times larger) than the spin period of the pulsar.

The latter effect allows a measurement of the individual masses of the components. One of the most important results in this paper is a detailed study of the conditions under which γ can be measured and its covariance with the variation of the projected semi-major axis, \dot{x} , in particular with the kinematic component of that term that arises inevitably from the proper motion of the system. This means that, in order to estimate the component masses of a wide binary system with the help of γ , we must take into account at least the effect of the proper motion. We do this in an economical and self-consistent way by sampling the quality (χ^2) of the timing fit for the full orbital orientation space (which consists of $\cos i$ and Ω). From this χ^2 map, we derive probabilistic distributions for $\cos i$, M_p and M_c . The median and 68.3% confidence limits of the mass distributions are given by $M_p = 1.25_{-0.06}^{+0.05} M_\odot$ and a companion mass of $M_c = 1.22_{-0.05}^{+0.06} M_\odot$.

The low mass of the MSP implies that the recycling process can be achieved with a relatively small amount of mass, $< 0.08 M_\odot$. We cannot use this number to estimate the efficiency of the recycling process (as done by, e.g., Antoniadis et al. 2012) because we do not know the mass and orbital properties of the original donor star.

The mass of the current companion implies the possibility that it is also a NS. This makes the system very similar to PSR J1807–2500B, located in the globular cluster NGC 6544. Both systems were very likely formed by exchange interactions in the core of the globular clusters where they are located, both are potential MSP - NS systems, but each could also be a MSP - massive WD system. Given the possibility that the companion is a NS, we have looked deeply for radio pulsations from the companion, but

none were found. Therefore, we cannot determine the nature of the companion with any certainty.

The measured masses imply, according to GR, that the time until gravitational-wave induced merger of ~ 463 Gyr, which is more than 30 times the Hubble time. It is to be expected, given the dense environment and the history of the system, that its interactions with other stars in the cluster will produce very significant changes in its orbital parameters (or even in the companion itself) on a timescale much shorter than the orbital decay timescale.

Future observations will refine the proper motion, which will allow us to measure precisely (and hopefully accurately) the velocity difference relative to the cluster. Such observations will also allow a confirmation (or not) of the anomalous orbital period derivative of the system.

ACKNOWLEDGEMENTS

A.R. and P.C.C.F. gratefully acknowledge financial support by the European Research Council, under the European Union’s Seventh Framework Programme (FP/2007-2013) grant agreement 279702 (BEACON) and continuing support from the Max Planck Society. A.R. thanks the Autonomous Region of Sardinia (RAS) for financial support through the Regional Law 7 August 2007 n. 7 (year 2015) “Highly qualified human capital”, in the context of the research project CRP 18 “General relativity tests with the Sardinia Radio Telescope” (P.I.: M. Burgay). We thank the staff of the GMRT for help with the observations. The GMRT is operated by the National Centre for Radio Astrophysics (NCRA) of the Tata Institute of Fundamental Research (TIFR), India. The National Radio Astronomy Observatory is a facility of the National Science Foundation operated under cooperative agreement by Associated Universities, Inc. S.M.R. is a CIFAR Senior Fellow and is supported by the NSF Physics Frontiers Center award 1430284. A.R. also thanks Caterina Tiburzi, Andrea Possenti, Cees Bassa and Kuo Liu for useful discussions. This research has made extensive use of NASA’s Astrophysics Data System (ADS).

REFERENCES

- Antoniadis J., van Kerkwijk M. H., Koester D., Freire P. C. C., Wex N., Tauris T. M., Kramer M., Bassa C. G., 2012, *MNRAS*, **423**, 3316
- Arzoumanian Z., et al., 2018, *ApJS*, **235**, 37
- Barker B. M., O’Connell R. F., 1975, *Phys. Rev. D*, **12**, 329
- Baumgardt H., Hilker M., 2018, *MNRAS*, **478**, 1520
- Blandford R., Teukolsky S. A., 1976, *ApJ*, **205**, 580
- Boshkayev K., Quevedo H., Zhami B., 2017, *MNRAS*, **464**, 4349
- Boyles J., Lorimer D. R., Turk P. J., Mnatsakanov R., Lynch R. S., Ransom S. M., Freire P. C., Belczynski K., 2011, *ApJ*, **742**, 51
- Cadelano M., Ransom S. M., Freire P. C. C., Ferraro F. R., Hessels J. W. T., Lanzoni B., Pallanca C., Stairs I. H., 2018, *ApJ*, **855**, 125
- Corongiu A., Kramer M., Stappers B. W., Lyne A. G., Jessner A., Possenti A., D’Amico N., Löhmer O., 2007, *A&A*, **462**, 703
- Damour T., Deruelle N., 1985, *Ann. Inst. Henri Poincaré Phys. Théor.*, Vol. 43, No. 1, p. 107 - 132, **43**, 107

Damour T., Deruelle N., 1986, *Ann. Inst. Henri Poincaré Phys. Théor.*, Vol. 44, No. 3, p. 263 - 292, [44, 263](#)

Damour T., Taylor J. H., 1991, [ApJ, 366, 501](#)

Damour T., Taylor J. H., 1992, [Phys. Rev. D, 45, 1840](#)

DeCesar M. E., Ransom S. M., Kaplan D. L., Ray P. S., Geller A. M., 2015, [ApJ, 807, L23](#)

Folkner W. M., Williams J. G., Boggs D. H., Park R. S., Kuchynka P., 2014, *Interplanetary Network Progress Report*, [196, 1](#)

Fonseca E., Stairs I. H., Thorsett S. E., 2014, [ApJ, 787, 82](#)

Freire P. C. C., 2013, in van Leeuwen J., ed., Vol. 291, *Neutron Stars and Pulsars: Challenges and Opportunities after 80 years*. pp 243–250 ([arXiv:1210.3984](#)), [doi:10.1017/S1743921312023770](#)

Freire P. C. C., Wex N., 2010, [MNRAS, 409, 199](#)

Freire P. C., Gupta Y., Ransom S. M., Ishwara-Chandra C. H., 2004, [ApJ, 606, L53](#)

Freire P. C. C., Ransom S. M., Gupta Y., 2007, [ApJ, 662, 1177](#)

Freire P. C. C., et al., 2011a, [Science, 334, 1107](#)

Freire P. C. C., et al., 2011b, [MNRAS, 412, 2763](#)

Freire P. C. C., et al., 2017, [MNRAS, 471, 857](#)

Gaia Collaboration et al., 2018, [A&A, 616, A12](#)

Gupta Y., et al., 2017, *Current Science*, 113, 707

Harris W. E., 1996, [AJ, 112, 1487](#)

Hessels J. W. T., Ransom S. M., Stairs I. H., Freire P. C. C., Kaspi V. M., Camilo F., 2006, [Science, 311, 1901](#)

Jacoby B. A., Cameron P. B., Jenet F. A., Anderson S. B., Murty R. N., Kulkarni S. R., 2006, [ApJ, 644, L113](#)

Johnson T. J., et al., 2013, [ApJ, 778, 106](#)

Kopeikin S. M., 1995, [ApJ, 439, L5](#)

Kopeikin S. M., 1996, [ApJ, 467, L93](#)

Lorimer D. R., Kramer M., 2004, *Handbook of Pulsar Astronomy*

Lynch R. S., Freire P. C. C., Ransom S. M., Jacoby B. A., 2012, [ApJ, 745, 109](#)

Manchester R. N., Hobbs G. B., Teoh A., Hobbs M., 2005, [AJ, 129, 1993](#)

Martinez J. G., et al., 2015, [ApJ, 812, 143](#)

Mereghetti S., Tiengo A., Esposito P., La Palombara N., Israel G. L., Stella L., 2009, [Science, 325, 1222](#)

Papitto A., et al., 2013, [Nature, 501, 517](#)

Peters P. C., 1964, [Physical Review, 136, 1224](#)

Prince T. A., Anderson S. B., Kulkarni S. R., Wolszczan A., 1991, [ApJ, 374, L41](#)

Ransom S. M., 2001, PhD thesis, Harvard University

Ransom S. M., 2008, in Vesperini E., Giersz M., Sills A., eds, *IAU Symposium Vol. 246, Dynamical Evolution of Dense Stellar Systems*. pp 291–300, [doi:10.1017/S1743921308015810](#)

Reddy S. H., et al., 2017, [Journal of Astronomical Instrumentation, 6, 1641011](#)

Robertson H. P., 1938, *Ann. Math.*, 38, 101

Shklovskii I. S., 1970, *Soviet Ast.*, [13, 562](#)

Splaver E. M., Nice D. J., Arzoumanian Z., Camilo F., Lyne A. G., Stairs I. H., 2002, [ApJ, 581, 509](#)

Stovall K., et al., 2018a, preprint, ([arXiv:1809.05064](#))

Stovall K., et al., 2018b, [ApJ, 854, L22](#)

Taylor J. H., 1992, *Philosophical Transactions of the Royal Society of London Series A*, [341, 117](#)

Taylor J. H., Weisberg J. M., 1982, [ApJ, 253, 908](#)

Verbunt F., Freire P. C. C., 2014, [A&A, 561, A11](#)

Weisberg J. M., Huang Y., 2016, [ApJ, 829, 55](#)

Wex N., Johnston S., Manchester R. N., Lyne A. G., Stappers B. W., Bailes M., 1998, [MNRAS, 298, 997](#)

van Straten W., Bailes M., 2003, in Bailes M., Nice D. J., Thorsett S. E., eds, *Astronomical Society of the Pacific Conference Series Vol. 302, Radio Pulsars*. p. 65

van Straten W., Demorest P., Osłowski S., 2012, *Astronomical Research and Technology*, [9, 237](#)

This paper has been typeset from a $\text{\TeX}/\text{\LaTeX}$ file prepared by the author.